Visual Analysis of the Relation Between Stiffness Tensor and the Cauchy-Green Tensor

Christian Blecha[1], Chiara Hergl[1], Thomas Nagel[2], and Gerik Scheuermann[1]

[1]Leipzig University, Germany
[2] Chair of Soil Mechanics and Foundation Engineering, Geotechnical Institute, Technische Universität Bergakademie Freiberg, Germany

Abstract

Stress and strain tensors, two well-known quantities in mechanical engineering, are linked through a fourth-order stiffness tensor, which is not considered by many visualizations due to its complexity. Considering an orthotropic material, the tensor naturally decomposes into nine known material properties. We used fiber surfaces to analyze a data set representing a biological tissue. A sphere is pushed into the material to confirm the mathematical link as well as the possibility to extract highly deformed regions even if only the stiffness tensor is available.

CCS Concepts

• ***Computing methodologies*** → *Simulation evaluation;* ***Scientific visualization;***

1. Introduction

Many visualization techniques exist for the stress and strain tensors from mechanical engineering. These two tensors are linked through a fourth-order three-dimensional stiffness tensor (see Equation 1), which has 81 coefficients, where 21 are independent. Despite its interest to engineers, not many visualizations can show this tensor. If an orthotropic material (a relevant material anisotropy type) is considered in its natural coordinate system, only nine independent coefficients remain. This means that the link between applied stress and resulting deformation results, very naturally, in a nine-dimensional coefficient space. Here, we show how these nine coefficients can be calculated and visualized using fiber surfaces. Furthermore, we show how highly deformed regions could be extracted only by using the stiffness tensor. This is of practical importance if elastography is used, e.g., as a medical imaging method measuring the stiffness of soft tissues using magnetic resonance.

2. Related Work

Up to this point, tensor visualization has received some attention. Especially second-order tensors were frequently considered. Regarding tensors in engineering and mechanics, the reader may consult the survey by Kratz et al. [KASH13] and the one by Hergl et al. [HBK*21]. Unlike the stress and strain tensor, higher-order tensors have rarely been visualized (notable exception: the stress gradient visualization by Zobel et al. [ZSS17]). The visualization of the fourth-order stiffness tensor is the subject of some works. Neeman et al. [NBJ*08] used the Kelvin mapping to generalize the spectral decomposition and visualized the eigentensor of the stretch part regarding the largest eigenvalue using a Reynold's glyph. Kriz et al. [KYHR05] calculated the plane waves of each tensor and visualized them by a three-dimensional hull. Another glyph was designed by Hergl et al. [HNKS19], where they used the deviatoric decomposition to calculate the symmetries of the material. The symmetry plane normals are the principal component of the designed glyph. Similar to this work, Zobel et al. [ZSS15] analyzed the link between two tensors, i.e., the stress and fiber orientation distribution tensor. They combined insights from both tensors into one glyph. One of the oldest and most known visualization technique are isosurfaces, which are the preimage of a point in a one-dimensional range. They were extended to higher dimensional ranges by Carr et al. [CGT*15] (2D), Raith et al. [RBN*19] (3D), and by Blecha et al. [BRP*20] (nD). Furthermore, Blecha et al. [BRS*19] showed that the fiber surfaces by Raith et al. [RBN*19] are not only a tensor visualization but rather a multivariate visualization technique. Multivariate visualization techniques are no new phenomena. For example, Fuchs and Hauser [FH09] wrote a survey in 2009 about multivariate visualization and reviewed which visualization techniques, mainly invented for scalars, vectors, or tensors could be used for multivariate data sets and what their advantages are. Furthermore, the importance of the development of multivariate visualization techniques was mentioned by several works [Car14, CLKH14, OP14]. One common visualization technique for multivariate data sets are scatterplot matrices [CLNL87], which were enhanced to continuous scatterplots by Bachthaler and Weiskopf [BW08]. Unfortunately, multiple marked regions inside scatterplot matrices have to be combined if more than two quantities should be constrained. Jankoway et al. [JH18] introduced feature level-sets as feature surfaces, where iso- and fiber surfaces form special cases. Compared to the n-dimensional fiber surfaces

DOI: 10.2312/evs.20211052

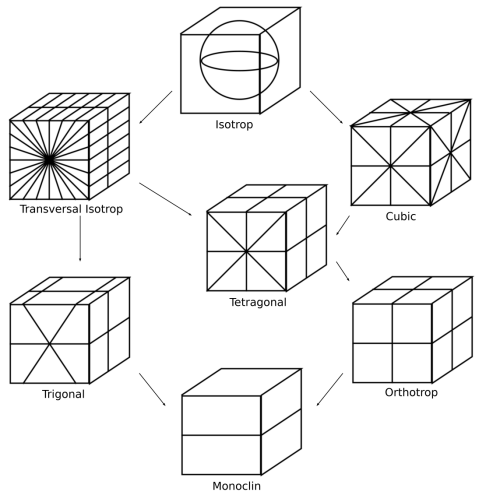

Figure 1: *Anisotropy classes of the stiffness tensor.*

by Blecha et al. [BRP*20], Jankoway et al. [JH18] and Raith et al. [RBN*19] only extract the surfaces and not the selected regions of interest.

3. Fundamentals

For the analysis of a tensor field, there are some fundamentals needed. A general introduction to tensor mathematics is given by Hergl et al. [HNS20]. This section will introduce the stiffness tensor and gives an overview of the rotation of this tensor in its natural coordinate system. The moduli of an orthotropic tensor can be read off the inverse of this rotated tensor. Analyses of biological materials often use formulations from the family of Ogden models [Ogd72]. In the sequel, a variant of the Ogden model, implemented into the open-source finite element software FEBio [EAW12], was used. Further information about the material model are given in the supplemental material.

3.1. Stiffness Tensor - Decomposition

The stiffness tensor $\mathcal{C}$ is a fourth-order three-dimensional tensor with the minor symmetries $C_{ijkl} = C_{jikl} = C_{ijlk}$ and, assuming hyperelasticity, the major symmetry $C_{ijkl} = C_{klij}$. It describes the relation between the stress tensor σ and the strain tensor ε, or their increments, through a linear mapping. In linear elastic materials for small strains, this relation is usually expressed as

$$\sigma = \mathcal{C} : \varepsilon. \tag{1}$$

For the variety of finite deformation and stress measures, corresponding stiffness tensors can be derived in the appropriate configurations.

The stiffness tensor can describe isotropy as well as different anisotropy types that are shown in Figure 1. The planes in the sketch describe the symmetry planes of the particular anisotropy type in a given point. A symmetry plane is given if the material properties fulfill the symmetry. For this work, just the symmetry types higher or equal to orthotropy are relevant because in the used model, the anisotropy is deformation-induced.

The tensor coefficients are highly dependent on the local coordinate system. Even if the coefficients are known, they may require further manipulation to link them to quantities of a certain physical meaning. Typically, engineers express the orthotropic stiffness tensor in its natural coordinate system. In this system, the stiffness tensor, describing an orthotropic linear elastic material, can be represented by its inverse using the Kelvin mapping [NGMK16]

$$\mathbf{C}_{\mathrm{K}}^{-1} = \begin{pmatrix} \frac{1}{E_1} & -\frac{\nu_{21}}{E_2} & -\frac{\nu_{31}}{E_3} & 0 & 0 & 0 \\ -\frac{\nu_{12}}{E_1} & \frac{1}{E_2} & -\frac{\nu_{32}}{E_3} & 0 & 0 & 0 \\ -\frac{\nu_{13}}{E_1} & -\frac{\nu_{23}}{E_2} & \frac{1}{E_3} & 0 & 0 & 0 \\ 0 & 0 & 0 & \frac{1}{2G_{23}} & 0 & 0 \\ 0 & 0 & 0 & 0 & \frac{1}{2G_{31}} & 0 \\ 0 & 0 & 0 & 0 & 0 & \frac{1}{2G_{12}} \end{pmatrix}, \tag{2}$$

where E_i are Young's moduli, ν_{ij} Poisson's ratios, and G_{ij} the shear moduli. Young's modulus describes the proportional relation between the stress and the strain for uniaxial stress states under linear elastic behavior. Poissons' ratio describes the expansion (or compression) in the direction perpendicular to the direction of loading. The shear modulus is a mechanical property that defines shear stress in relation to the shear strain.

As described before, the stiffness tensor is usually not given in natural coordinates at all positions in the field. To calculate the moduli from Equation 2, a rotation into this coordinate system is required at each considered position. For this rotation, we follow the calculations from Zou et al. [ZTL13]. First, the deviatoric decomposition of the stiffness tensor is calculated using

$$\mathcal{C} = \mathcal{D} + 6\mathbf{s}(\mathbf{I}\mathbf{D}^1) + 3\mathbf{s}(\mathbf{I}\mathbf{I}d^1) + \phi(\mathbf{D}^2) + \frac{1}{2}\phi(\mathbf{I}d^2). \tag{3}$$

The stiffness tensor can be described by the fourth-order deviator $\mathcal{D}$, the two second-order deviators $\mathbf{D}^1$ and $\mathbf{D}^2$, the two zeroth-order deviators d^1 and d^2, and the second-order identity tensor $\mathbf{I}$. Each of the deviators can be described by a set of vectors, called multipoles, and scalars using the symmetrization operator $\mathbf{s}(\cdot)$ by

$$\mathbb{D} = a\,\mathbf{s}(\mathbf{n}_1 \otimes \cdots \otimes \mathbf{n}_q). \tag{4}$$

Thus, the second step is the identification of the multipoles for each deviator to identify its anisotropy type. More detailed information about the multipole decomposition is given by Hergl et al. [HNS20]. A second-order deviator is orthotropic if its two multipoles do not vanish and are not equal. Following this, the symmetry plane normals are given by the two intersecting lines of the multipoles and the orthogonal one. A fourth-order deviator is orthotropic if its four multipoles do not vanish and can be mirrored by three orthogonal planes. The symmetry plane normals of the original tensor are given by the intersection of the sets of symmetry plane normals of the deviators.

The stiffness tensor in its local coordinate system can be identified by a rotation of the original tensor. The rotated tensor $\mathcal{C}^R$ of the stiffness tensor $\mathcal{C}$ is given by

$$C^R_{ijkl} = R_{im}R_{jn}R_{ko}R_{lp}C_{mnop}, \tag{5}$$

where **R** is the well-known rotation matrix. Further information, as well as an example, are provided in the supplemental material.

4. Visual Analysis using nD-Fiber Surfaces

The analysis of multivariate data is still a challenging task. Especially as the number of considered variables increases because the technique allows simulating increasingly complex processes and materials. The analysis of the stiffness tensor for orthotropic materials (It could also be applied to isotropic, transversal isotropic, and cubic materials.) naturally leads to a nine-dimensional coefficient space, which would lead to 45 plots in a scatterplot matrix.

4.1. Algorithm and Data Set

We reduced the needed complexity by using n-dimensional fiber surfaces [BRP*20] because they extend a well-known visualization technique for domain and visualization experts. Regions of interest are selected through the intersection of multiple n-dimensional half-spaces (in the following called hyper planes), represented by a n-dimensional normal and a distance to an origin. These two elements are used to calculate the intersection of each hyper plane with each tetrahedron of the grid. Thereby, the algorithm triangulates the intersection areas, which are the fiber surfaces, and splits the remaining polyhedron, which lies inside the half-space, into tetrahedra. We refer to the work by Blecha et al. [BRP*20] for more information on the extraction algorithm.

We used a simple data set representing a block of an initially isotropic material into which a sphere is pushed so that the complexity of the process is not increased or masked by a complex geometry. Due to symmetries, only a quarter of this block is modeled. The process of indentation is represented by multiple time steps, starting with the undeformed block. Among other variables, the simulation calculated the stiffness tensor and the right Cauchy-Green tensor. Deformation leads to the development of different principal values of the right Cauchy-Green tensor, which in turn leads to the emergence of anisotropy in the material due to its deformation-dependent nonlinearity. For the analysis, the nine coefficients of the orthotropic stiffness tensor were calculated at each grid vertex using the results of Section 3. Additionally, we calculated the three eigenvalues of the right Cauchy-Green tensor.

4.2. Nine-dimensional Overviews

In the beginning, we created an overview visualization of all nine coefficients of the orthotropic stiffness tensor. In particular, they can be categorized into three Young's moduli, three shear moduli, and three Poisson ratios. This natural fragmentation into multiple triplets underlines the applicability of the algorithm by Blecha et al. [BRP*20] because they visualize the attribute space as combination of multiple three-dimensional subspaces. It is mentioned here again that parameters from linear small-deformation settings are used to make the interpretation of the stiffness tensor entries more accessible. The first step showed the distribution of each variable in the spatial domain. This means to push one hyper plane per variable through its range of all occurring values and to extract the corresponding fiber surfaces. Figure 2 can be split semantically into four super parts [1_x_1, ..., 4_x_4]. Each of them shows either the extracted fiber surfaces of one triplet or the position of the intersecting hyper planes [4_x_4]. Each super part is split into four subparts [y_1, ..., y_4], showing either the extracted fiber surfaces of one variable of the subspace in the spatial domain (separated by color and shown with multiple viewing angles) or multiple viewing angles of the corresponding three-dimensional subspace. This was done over all time steps and combined into a video showing the extraction of fiber surfaces cutting of regions with increasing values (see the supplemental material). The overview visualization shows that higher Young's moduli are located in the lower right corner of the physical block, where the sphere is pressed into the material the farthest. This applies to the shear moduli and the Poisson's ratios in a similar way. Our domain expert was also sold on this visualization style as he could see and compare multiple distributions at the same time.

4.3. 12-dimensional Filters

Furthermore, our expert mentioned his interest in a comparison of regions with high stiffness measures with the eigenvalues of the right Cauchy-Green tensor inside these areas because this would enable the possibility to extract highly deformed regions if elastography is used to measure elastic properties of the material. The first step was to add the three eigenvalues of this tensor to the coefficient space, which lead to a 12-dimensional space. Following this, one hyper plane was defined to extract regions with higher Young's moduli (represented by a blue plane in the lower left part [3_x_3] of Figure 3). In the three other super parts of Figure 3, we visualized the distribution of the shear moduli [1_x_1], the Poisson's ratios [2_x_2], and the eigenvalues of the right Cauchy-Green tensor (GEV_i) [5_x_5] inside the extracted region with high Young's moduli. The coefficient subspaces show the distribution of values of the filtered space in dark and of the not filtered space in light colors. This step could not be done with the three-dimensional fiber surfaces by Raith et al. [RBN*19] because they could not filter the data and show the remaining part inside the other dimensions. Considering regions with increasing Young's moduli, our domain expert ascertained that these regions coincide with higher values in all other subspaces, especially with the eigenvalues of the right Cauchy-Green tensor. This means that highly deformed regions can not only be extracted by looking directly at a given deformation quantity but also by looking at regions characterized by high stiffness values. The domain expert mentioned that this is a consequence of the mathematical link described by the used Ogden material model and that highly deformed regions could also be identified if only the stiffness tensor and not a deformation quantity is accessible.

4.4. Spatial Filters

During the analysis of the 12-dimensional space, we investigated some irregularities inside the different subspaces. Considering the video in the supplemental material, a fold-down lug could be identified in the middle of the subspaces of the Poisson ratios and the eigenvalues of the right Cauchy-Green tensor. At first, a new combination of hyper planes was used to separate this lug from the remaining values, which lead to a corresponding fiber surface in the lower part of the spatial domain. Our domain expert mentioned that

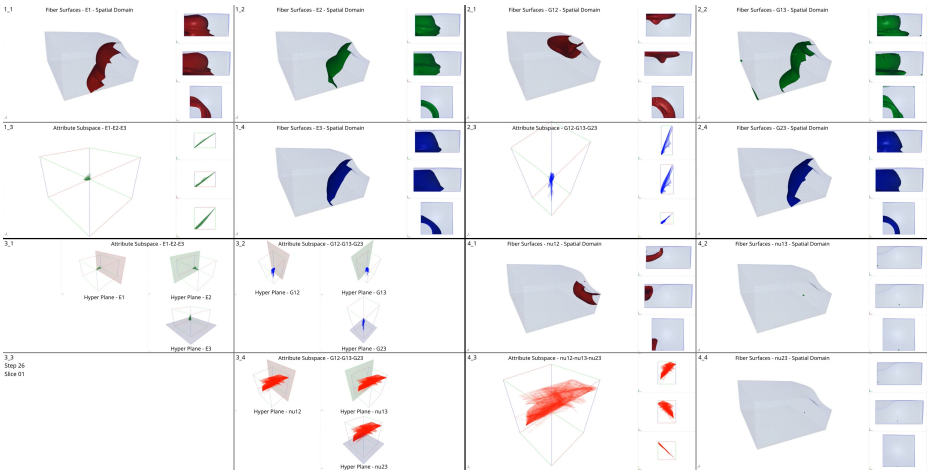

Figure 2: *Overview visualization showing fiber surfaces extracted from the subspace of Young's moduli [1_x_1], shear moduli [2_x_2], Poisson ratios [4_x_4], and the corresponding hyper planes used for the fiber surface extraction for each variable in the lower left part [3_x_3].*

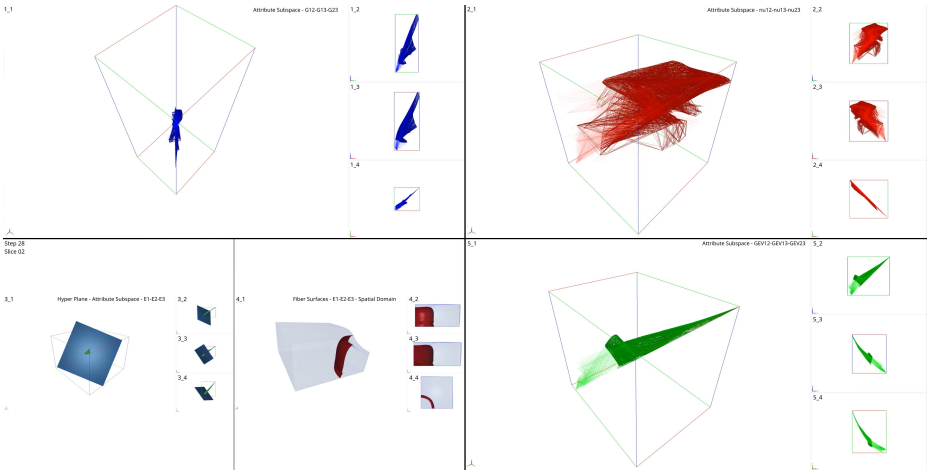

Figure 3: *Overview visualization showing the distribution of variables inside regions with high Young's moduli [3_x_3]. The dark colors show the variable distributions of the filtered regions compared to the distribution of the variables of the whole data set in light colors inside the subspaces of shear moduli [1_x_1], Poisson ratios [2_x_2], and the eigenvalues of the right Cauchy-Green tensor [5_x_5]. The used hyper plane for the filtering inside the subspace of the Young's modulus [3_x_3] and the corresponding fiber surface inside the spatial domain [4_x_4] are shown in the lower-left corner.*

this could be due to boundary conditions because in the simulation, the block was fixed on the bottom. In a second step, we used a hyper plane in the spatial domain to extract this lower area and to analyze the distribution of the variables in this region. This proved the hypothesis that the lug exists due to the imposed boundary conditions.

5. Conclusion and Future Work

We used the fiber surface algorithm by Blecha et al. [BRP*20] and applied it on a 9- and a 12-dimensional coefficient space representing the coefficients of the stiffness tensor and the right Cauchy-Green tensor of an orthotropic material. We showed that the algorithm could be used to create overview visualizations to analyze the distribution of multiple variables in the same way as scatter plot matrices, by a simultaneous reduction of the used plots. Additionally, the algorithm can be used to filter and refine the used data set in the first step and analyze the distributions of the remaining variables afterward. This was used to illustrate the link between the stiffness and the right Cauchy-Green tensor, enabling the possibility to extract regions with high deformations even if no deformation quantity but a stiffness tensor were given. The filtering could also be used to investigate the effect of boundary conditions.

Future work could, for example, be the development of visualization techniques for the attribute space plots because they suffer very much from self-overlapping.

References

[BRP*20] BLECHA C., RAITH F., PRÄGER A. J., NAGEL T., KOLDITZ O., MASSMANN J., RÖBER N., BÖTTINGER M., SCHEUERMANN G.: Fiber surfaces for many variables. *Computer Graphics Forum 39*, 3 (2020), 317–329. URL: https://onlinelibrary.wiley.com/doi/abs/10.1111/cgf.13983, arXiv:https://onlinelibrary.wiley.com/doi/pdf/10.1111/cgf.13983, doi:https://doi.org/10.1111/cgf.13983. 1, 2, 3, 4

[BRS*19] BLECHA C., RAITH F., SCHEUERMANN G., NAGEL T., KOLDITZ O., MASSMANN J.: Analysis of Coupled Thermo-Hydro-Mechanical Simulations of a Generic Nuclear Waste Repository in Clay Rock Using Fiber Surfaces. In *2019 IEEE Pacific Visualization Symposium (PacificVis)* (April 2019), pp. 189–201. 1

[BW08] BACHTHALER S., WEISKOPF D.: Continuous scatterplots. *IEEE Transactions on Visualization and Computer Graphics 14*, 6 (2008), 1428–1435. doi:10.1109/TVCG.2008.119. 1

[Car14] CARR H.: Feature analysis in multifields. In *Scientific Visualization*. Springer, 2014, pp. 197–204. 1

[CGT*15] CARR H., GENG Z., TIERNY J., CHATTOPADHYAY A., KNOLL A.: Fiber Surfaces: Generalizing Isosurfaces to Bivariate Data. *Computer Graphics Forum 34*, 3 (2015), 241–250. 1

[CLKH14] CHUNG D. H., LARAMEE R. S., KEHRER J., HAUSER H.: Glyph-based multi-field visualization. In *Scientific Visualization*. Springer, 2014, pp. 129–137. 1

[CLNL87] CARR D. B., LITTLEFIELD R. J., NICHOLSON W. L., LITTLEFIELD J. S.: Scatterplot matrix techniques for large n. *Journal of the American Statistical Association 82*, 398 (1987), 424–436. URL: https://doi.org/10.1080/01621459.1987.10478445, arXiv:https://doi.org/10.1080/01621459.1987.10478445, doi:10.1080/01621459.1987.10478445. 1

[EAW12] ELLIS B., ATESHIAN G., WEISS J.: Febio: finite elements for biomechanics. *J Biomech Eng 134*, 1 (2012), 5–11. 2, 6

[FH09] FUCHS R., HAUSER H.: Visualization of multi-variate scientific data. In *Computer Graphics Forum* (2009), vol. 28, Wiley Online Library, pp. 1670–1690. 1

[HBK*21] HERGL C., BLECHA C., KRETZSCHMAR V., RAITH F., GÜNTHER F., STOMMEL M., JANKOWAI J., HOTZ I., NAGEL T., SCHEUERMANN G.: Visualization of tensor fields in mechanics. doi:https://doi.org/10.1111/cgf.14209. 1

[HNKS19] HERGL C., NAGEL T., KOLDITZ O., SCHEUERMANN G.: Visualization of symmetries in fourth-order stiffness tensors. In *2019 IEEE Visualization Conference (VIS)* (2019), IEEE, pp. 291–295. 1

[HNS20] HERGL C., NAGEL T., SCHEUERMANN G.: An introduction to the deviatoric tensor decomposition in three dimensions and its multipole representation. *arXiv preprint arXiv:2009.11723* (2020). 2

[JH18] JANKOWAI J., HOTZ I.: Feature level-sets: Generalizing iso-surfaces to multi-variate data. *IEEE transactions on visualization and computer graphics* (2018). 1, 2

[KASH13] KRATZ A., AUER C., STOMMEL M., HOTZ I.: Visualization and analysis of second-order tensors: Moving beyond the symmetric positive-definite case. In *Computer Graphics Forum* (2013), vol. 32, Wiley Online Library, pp. 49–74. 1

[KYHR05] KRIZ R., YAMAN M., HARTING M., RAY A.: Visualization of zeroth, second, fourth, higher order tensors, and invariance of tensor equations. *Computers and Graphics 21*, 6 (2005), 1–13. 1

[NBJ*08] NEEMAN A. G., BRANNON R., JEREMIĆ B., VAN GELDER A., PANG A.: Decomposition and visualization of fourth-order elastic-plastic tensors. In *Proceedings of the Fifth Eurographics/IEEE VGTC conference on Point-Based Graphics* (2008), Eurographics Association, pp. 121–128. 1

[NGMK16] NAGEL T., GÖRKE U.-J., MOERMAN K. M., KOLDITZ O.: On advantages of the Kelvin mapping in finite element implementations of deformation processes. *Environmental Earth Sciences 75*, 11 (jun 2016), 937. doi:10.1007/s12665-016-5429-4. 2

[Ogd72] OGDEN R. W.: Large deformation isotropic elasticity: on the correlation of theory and experiment for compressible rubberlike solids. *Proceedings of the Royal Society of London. Series A, Mathematical and Physical Sciences* (1972), 567–583. 2, 6

[OP14] OBERMAIER H., PEIKERT R.: Feature-based visualization of multifields. In *Scientific Visualization*. Springer, 2014, pp. 189–196. 1

[RBN*19] RAITH F., BLECHA C., NAGEL T., PARISIO F., KOLDITZ O., GÜNTHER F., STOMMEL M., SCHEUERMANN G.: Tensor Field Visualization using Fiber Surfaces of Invariant Space. *IEEE Transactions on Visualization and Computer Graphics 25*, 1 (Jan 2019), 1122–1131. 1, 2, 3

[ZSS15] ZOBEL V., STOMMEL M., SCHEUERMANN G.: Feature-based tensor field visualization for fiber reinforced polymers. In *2015 IEEE Scientific Visualization Conference (SciVis)* (2015), IEEE, pp. 49–56. 1

[ZSS17] ZOBEL V., STOMMEL M., SCHEUERMANN G.: Visualizing gradients of stress tensor fields. In *Modeling, Analysis, and Visualization of Anisotropy*. Springer, 2017, pp. 65–81. 1

[ZTL13] ZOU W.-N., TANG C.-X., LEE W.-H.: Identification of symmetry type of linear elastic stiffness tensor in an arbitrarily orientated coordinate system. *International Journal of Solids and Structures 50*, 14-15 (2013), 2457–2467. 2